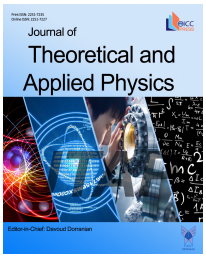

Volume 18, Issue 5, 182468 (1-10)

Journal of Theoretical and Applied Physics (JTAP)

https://dx.doi.org/10.57647/j.jtap.2024.1805.68

Synthesis, characterization and evaluations of structural, morphological and magnetic studies of yttrium doped Ni-Zn nano-ferrites via sol-gel method

Paramesh Donta*

Department of Physics, Sreenidhi Institute of Science and Technology, (Autonomous), Hyderabad, Telangana State, India.

***Corresponding author:** paramphd2009@gmail.com

Original Research

Received:
17 July 2024
Revised:
18 September 2024
Accepted:
27 September 2024
Published online:
30 October 2024

Abstract:

The yttrium-doped Ni-Zn ferrite of $Ni_{0.4}Zn_{0.6}Y_xFe_{2-x}O_4$ ($x = 0.0$, 0.03, 0.06, 0.09 and 0.12) nanoparticles was routed through sol-gel to examine the structural and magnetic. XRD authorized the establishment of a single-phase spinal structure and it was noticed that crystallite size (20.14 nm – 35.18 nm), lattice constant (8.369 $\AA$ – 8.424 $\AA$), jump lengths (L_A is from 3.635 $\AA$ – 3.651 $\AA$ and L_B is from 2.963 $\AA$ – 2.976 $\AA$) and unit cell volume (591.86 $\AA^3$ to 599.29 $\AA^3$) were increased with yttrium substitution. The density and porosity of the samples considerably varied with yttrium substitution. FESEM confirmed the morphology of the samples and EDX spectrographs were estimated the elemental compositions. The saturation magnetization (29.19 − 19.89 emu/g), remanence (16.79 − 11.63 emu/g), coercivity (206 – 56 Oe) and magnetic moment (1.24 – 0.86 A-m^2) were maintained the decrease trend with yttrium substitution.

Keywords: Sol-gel; XRD; FESEM and VSM analysis

1. Introduction

Nanoparticles research is a fast-developing zone with an extensive variety of possible applications in numerous domains such as the optical, biomedical, and electronic industries. The fabulous interest in the science and technology of nanostructures is highly inspired because of their physical and chemical properties which change amazingly when compared with their bulk form. Spinel ferrites are remarkable resources due to their extensive range of uses in the present era of science and technology. Mostly, they have attracted substantial interest in research due to their outstanding structural and electro-magnetic properties [1]. These substances have remarkable magnetic and dielectric properties as well as mechanical and chemical stability, especially at low frequencies [2]. Another flexibility of these structures is that their magnetic properties can be easily manageable and altered to be implemented for practical applications [3]. Ferrites are basically ferromagnetic oxide resources that are highlighted for their enormous applications in modern society and in different research fields. Polycrystalline ferrite materials are well-known for their properties like chemical stability, less magnetic loss, high permeability, high resistivity and low cost. Due to these properties, they are employed in electronic field to shape microwave devices, multilayer chips, transformers and electric generator storage devices [4]. Mostly, the polycrystalline ferrite properties depend on various constraints such as their preparation routes, thermal conditions, pH values, sintering conditions and cation distributions. The magnetic properties of the materials are tremendously dependent on the cation distribution among the *A* and *B*-sites [5]. In the material lattice, *A*-site ions may magnetize in a particular direction and *B*-site ions will magnetize in the opposite direction. Hence, the value of magnetization was not equal, which results in a net spontaneous magnetization. The structural studies play a vital role in determining the chemical and physical properties of the sample. As a result, a complete investigation of the structure of materials is reasonably significant to recognize the various changes in the properties of the material [6]. Yttrium nanoparticles have potential electrical, magnetic, optical, catalytic and biomedical applications. Such magnetic and ceramic additives improve the strength of the aluminium and magnesium alloys, microwave filters in radar, cata-

lysts, lasers as YAG (Yttrium-Aluminium Garnet), oxygen sensors in automobile exhaust systems, manufacturing in superconductors. Yttrium nano particles also used as solid electrolyte, coatings, nanowires, nano-fibers, textiles, bio imaging, used as a phosphor in various applications like fluorescent lamps, CRT and plasma displays, LEDs, electrodes, electronic filters, production of synthetic garments, used to manufacture infrared layers [7, 8]. As per the literature it came to know that many researchers were studied the effect of trivalent substitution in ferrites to strengthen their structural, magnetic and transport properties.

Several researchers are focused on Ni-Zn ferrite resistivity, but they are also eager to enhance their magnetic properties in an acceptable manner. S. Chakrabarty et al. reported the enhanced electrical resistivity and coercivity of yttrium doped nano particles have mostly been cited as justification for their promising application in microwave devices and high density recording medium. Rezlescu et al. reported that the Ni–Zn ferrites electrical and magnetic features may be affected by the rare earths minor substitution of Fe ions. As a result of their improved electrical properties, the yttrium-substituted Ni-Zn ferrites used in resonant wireless charging, high frequency power applications, high frequency systems in communication, defence and medical applications as well as EMI shielding materials to protect electronic devices from electromagnetic interference. The two main techniques for creating nanoparticles are top-down and bottom-up. Whereas atoms are first synthesized into clusters and then into nanoparticles in the bottom-up approach, the bulk material is transformed into powder and then nanoparticles in the top-down method. Typically, physical, chemical, and biological techniques are used to create materials that are nano scale. Physical processes such as ball milling, laser ablation, spray pyrolysis, ion beam lithography (IBL), electron beam lithography (EBL), traditional ceramic or solid-state reaction, etc. are used to create nanomaterials. The chemical techniques include phytochemical, solvothermal, sol-gel auto combustion, co-precipitation, sol-gel, pyrolysis and sonochemical processes. Thus, powder forms of nano-crystalline ferrites are created by a variety of methods and every method is having its own benefits. And the properties of the ferrites are heavily influenced by the process of preparation and as well as the composition.

A. Guadagnini et.al and N.S. Awwad et. al was reported that the laser ablation method has a many benefits such as accuracy, speed, compatibility with many materials, low damage, absence of chemicals and mechanical force, computerized interface control, environmental friendliness, and cost effectiveness. Additionally, it can be used for a wide range of tasks, including bulk metal analysis, soil analysis, drilling small areas successfully, specified holes and cutting through hard materials to produce thin films or nanoparticles. The sol-gel approach was selected by the author because to its ability to function at low temperatures, its affordability, and its ability to manage the material's texture, chemical composition, morphology, biocompatibility, and doping process. In addition to producing thin films with uniform thickness and regulated quality, this process yields high purity products. Sol-gel coatings possess excellent mechanical, chemical, and thermal stability and are inorganic. In this article the author also carefully synthesized and systematically scrutinized the influence of yttrium on the structural and magnetic analysis of Ni-Zn nanoferrite samples. The novelty of this article is to explore a new area for enlightening the physical properties. In this article, the crystallite sizes are reported approximately 20 nm to 30 nm, usually small crystallite sizes of ferrites employed in making the switching devices. The coercivity values lay between 56 Oe 206 Oe hence, the high coercivity value of ferrites is used in high-density magnetic recording devices.

2. Experimental details

2.1 Synthesis

Yttrium-substituted Ni-Zn ferrite nanoparticles of $Ni_{0.4}Zn_{0.6}Y_xFe_{2-x}O_4$ ($x = 0.0$, 0.03, 0.06, 0.09, and 0.12) were prepared through the sol-gel auto-combustion technique. According to the stoichiometric ratio, highly pure raw materials were used: analytical grade (AR) materials such as nickel nitrate ($Ni(NO_3)_2.6H_2O$), zinc nitrate ($Zn(NO_3)_2.6H_2O$), yttrium nitrate ($Y(NO_3)_3.6H_2O$), ferric nitrate ($Fe(NO_3)_3.9H_2O$) and citric acid ($C_6H_8O_7.H_2O$) all from Merck with 99% purity. These stoichiometric chemical reagents are put one by one into 25 mL of triple-distilled water and stirred on a magnetic stirrer until all the chemicals can dissolve in it. Now heat the nitrate mixture up to 60 °C on a magnetic stirrer then add the citric acid in a 3:1 molar ratio and stir the complex citrate solution for another 30 minutes at 80 °C. At this point, ammonia is added drop by drop to the complex citrate solution to keep the pH value at 7 and then the temperature of the magnetic stirrer is raised to 300 °C to get a gluey gel that encounters auto-combustion. The obtained powder of ferrite was sintered at a constant 600 °C for 5 hours and ground into a fine powder. The sol-gel synthesis flow chart was shown in Fig. 1.

2.2 Sample characterization

The XRD was studied by Phillips X'Pert XRD with CuKα wavelength (λ) of 1.5406 $\mathring{A}$, 2θ is taken in between 20° – 70° over a step value of 0.02° with a scan rate of 2°/minute at Osmania University, Hyderabad, India. The FESEM morphology was traced out by Carl Zeiss Microscopy GmbH, Germany at ARCI, Balapur, Hyderabad, India. A VSM magnetometer used to measure the hysteresis loops and magnetic characteristics at −20 KOe to +20 KOe at ARCI, Chennai-India.

3. Results and discussion

3.1 XRD study

XRD was studied to search for the properties of $Ni_{0.4}Zn_{0.6}YxFe_{2-x}O_4$ ($x = 0.0$, 0.03, 0.06, 0.09, and 0.12) ferrite nanoparticles. The peaks (111), (220), (311), (222), (400), (422), (511), and (440) represent the cubic spinel structure without impurity and homogeneity of samples [9], shown in Fig. 2 (a). The obtained XRD pattern was absolutely sinks with the Fd3m group and JCPDS card no. 89-2355 [10]. It was noticed that the peak positions of

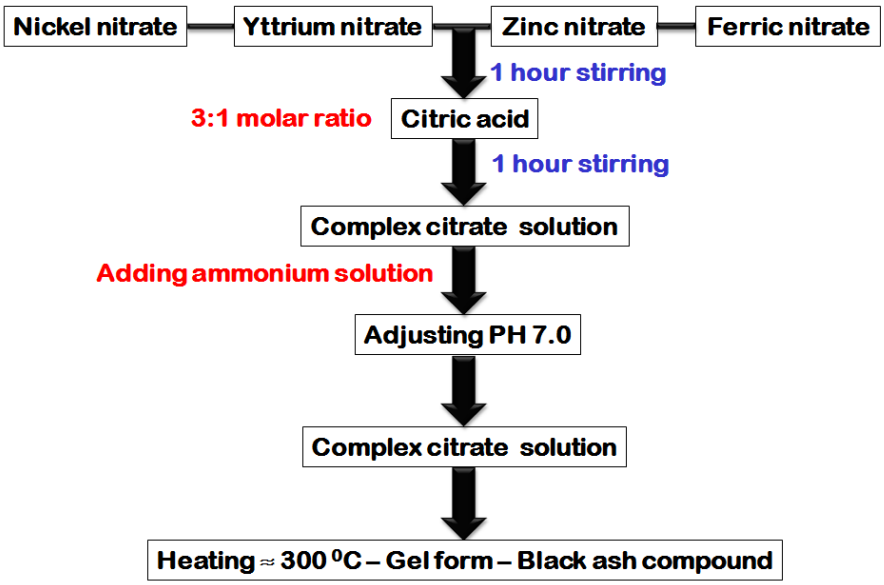

Figure 1. Flow chart of $Ni_{0.4}Zn_{0.6}Y_xFe_{2-x}O_4$ ($x = 0.0$, 0.03, 0.06, 0.09 and 0.12) ferrite nanoparticles via sol-get technique.

the (311) plane shifted towards the lower 2θ angle shown in Fig. 2 (b), which indicates a rise in lattice parameters with Y^{3+} ion substitution [11]. The average crystallite sizes determined by Debye-Scherer equation as follows

$$t = \frac{0.9\lambda}{\beta \cos\theta} \tag{1}$$

where, λ-wavelength (1.5405 $\AA$), θ-angle of the Bragg diffraction and β-full width at half maximum of intensive peak.

Lattice parameters esteemed by

$$a = d\sqrt{h^2 + k^2 + l^2} \tag{2}$$

where d-inter planar distance, a-lattice parameter and h, k, l-Miller Indices.

The L_A and L_B values were estimated with the help of Eqs. (3) & (4)

$$L_A = \frac{\sqrt{3}}{4}a \tag{3}$$

$$L_B = \frac{\sqrt{2}}{4}a \tag{4}$$

where, L_A – A-site length (Tetrahedral), L_B – B-site length (Octahedral) and a – Lattice constant.

The composition response with crystallite size, lattice constant, cell volume and jump lengths are shown in Figs. 3, 4, and 5. The crystallite sizes increased from 20.14 nm to 35.18 nm and the lattice constants also increased from 8.396 $\AA$ to 8.431 $\AA$ with yttrium substitution. This is caused by the replacement of a greater radius of Y^{3+} (0.95 $\AA$) in place of a smaller radius of Fe^{3+} ions (0.67 $\AA$) in the octahedral site. The increase in the lattice constant values is also confirmed owing to the variation of the surface-to-volume ratio [12]. The cell volume is also noticed to increase from 591.86 ($\AA^3$) to 599.29 ($\AA^3$) with yttrium substitution because it is directly proportional to lattice parameter values [13]. This enlargement of unit cell volume endorses the successful and

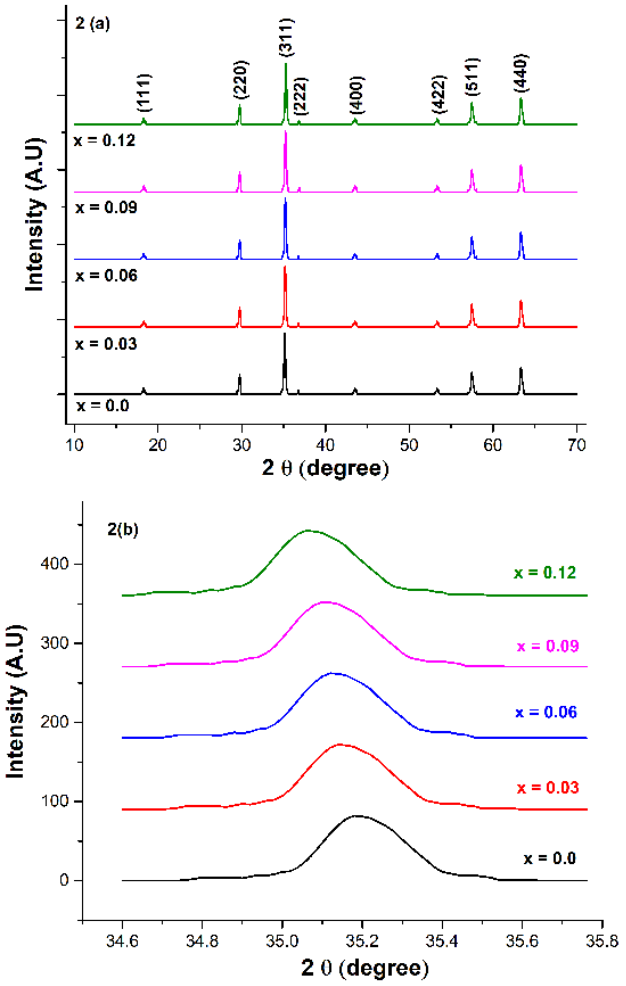

Figure 2. (a) XRD of $Ni_{0.4}Zn_{0.6}Y_xFe_{2-x}O_4$ ($x = 0.0$, 0.03, 0.06, 0.09 and 0.12) ferrite nanoparticles, (b) 311 peak of $Ni_{0.4}Zn_{0.6}Y_xFe_{2-x}O_4$ ($x = 0.0$, 0.03, 0.06, 0.09 and 0.12) ferrite nanoparticles .

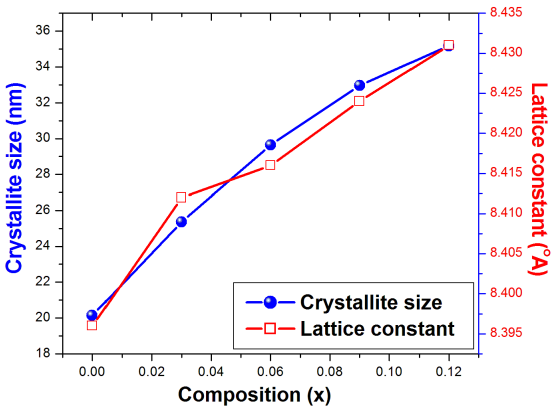

Figure 3. Composition versus crystallite size and lattice constant of $Ni_{0.4}Zn_{0.6}Y_xFe_{2-x}O_4$ ($x = 0.0$, 0.03, 0.06, 0.09 and 0.12) ferrite nanoparticles.

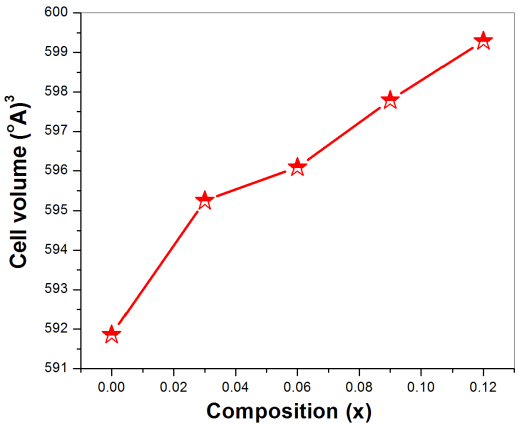

Figure 4. Composition versus Cell volume of $Ni_{0.4}Zn_{0.6}Y_xFe_{2-x}O_4$ ($x = 0.0$, 0.03, 0.06, 0.09 and 0.12) ferrite nanoparticles.

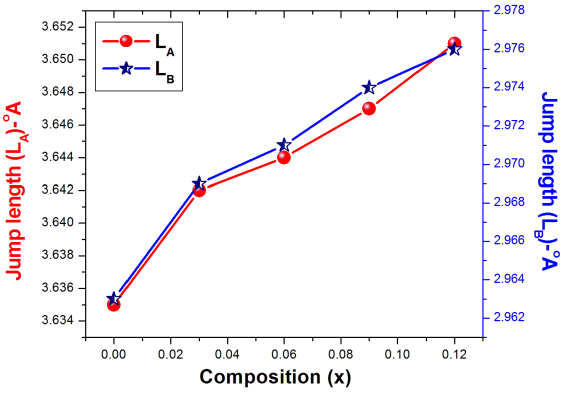

Figure 5. Composition versus Jump lengths (L_A and L_B) of $Ni_{0.4}Zn_{0.6}Y_xFe_{2-x}O_4$ ($x = 0.0$, 0.03, 0.06, 0.09 and 0.12) ferrite nanoparticles.

perfect substitution of larger Y^{3+} ions for smaller Fe^{3+} ions [14], A. Ahad et al. reported similar findings. It is also observed that the jump lengths (L_A and L_B) increased with the Y^{3+} ion substitution, owing to the fact that the increase in lattice constant values hints at a resulting decrease in the L_A and L_B values [15]. Garima Rana et al. obtained similar results. The corresponding values of crystallite size, lattice constants, jump lengths, and cell volume are posted in Table 1. The porosity, X-ray, and bulk density were evaluated through Eqs. (5), (6), and (7).

$$\rho_x = \frac{8M}{Na^3} \tag{5}$$

where, ρ_x– X-ray density, M–Molecular weight, N–Avogadro number, a–Lattice constant.

$$\rho_B = \frac{m}{\pi r^2 t} \tag{6}$$

where, ρ_B-bulk density, m–pellet mass, r–pellet radius, t–pellet thickness.

$$P = 1 - \frac{\rho_B}{\rho_x} \tag{7}$$

where, P–Porosity, ρ_B–bulk density, ρ_x– X-ray density. The electrical and magnetic properties of nano ferrites are remarkably controlled by their density, along with several other aspects like molecular weight and lattice parameters [16]. Table 1 indicates that the lattice parameters were increased from 8.396 $\AA$ to 8.431 $\AA$. The X-ray density of ferrite samples also increased from 5.334 g/cm^3 to 5.356 g/cm^3 [17, 18]. X-ray density is usually higher than bulk density because of the existence of pores in the samples during the sintering procedure and also because the prepared samples may have small fractures, gaps, and voids inside the lattice [19]. Further, it is also witnessed that the bulk density enlarged and porosity declined with Y^{3+} ion substitution; this is due to the fact that bulk density and porosity were inversely proportional to each other [20], similar reports were presented by K. Vani et al. The composition versus density and molecular weight of the sample and porosity were shown in Figs. 6 and 7 respectively and correspond to all values posted in Table 2.

3.2 FESEM and EDX study

The surface morphology of the ferrite materials can be investigated using SEM/FESEM. The presence of doping

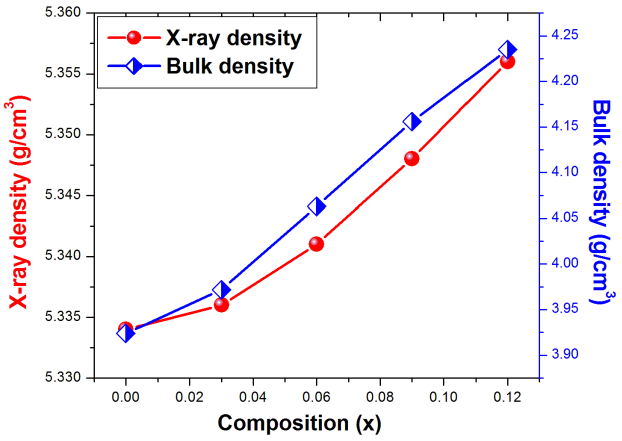

Figure 6. Composition versus X-ray density and bulk density of $Ni_{0.4}Zn_{0.6}Y_xFe_{2-x}O_4$ ($x = 0.0$, 0.03, 0.06, 0.09 and 0.12) ferrite nanoparticles.

Table 1. Composition (x) versus average crystallite size (t), lattice constant (a), jump lengths (L_A and L_B) and average cell volume of $Ni_{0.4}Zn_{0.6}Y_xFe_{2-x}O_4$ ($x = 0.0$, 0.03, 0.06, 0.09 and 0.12) ferrite nanoparticles.

Composition (x)	$x = 0.0$	$x = 0.03$	$x = 0.06$	$x = 0.09$	$x = 0.12$
Crystallite size (t-nm)	20.14	25.37	29.64	32.97	35.18
Lattice Constant (a)-Å	8.396	8.412	8.416	8.424	8.431
Jump Length (L_A)-Å	3.635	3.642	3.644	3.647	3.651
Jump Length (LB) -Å	2.963	2.969	2.971	2.974	2.976
Cell Volume $(Å)^3$	591.86	595.25	596.09	597.79	599.29
Average Cell Volume	XRD			596.05	
	JCPDS card no. 89-2355			591.86	

Table 2. Composition (x) versus molecular weight of the sample, X-ray density (ρ_x), bulk density (ρ_B), porosity (%) of $Ni_{0.4}Zn_{0.6}Y_xFe_{2-x}O_4$ ($x = 0.0$, 0.03, 0.06, 0.09 and 0.12) ferrite nanoparticles.

Composition (x)	$x = 0.0$	$x = 0.03$	$x = 0.06$	$x = 0.09$	$x = 0.12$
Molecular Weight (g/mole)	237.68	238.67	239.66	240.65	241.64
X-ray density (ρ_x) (g/cm^3)	5.334	5.336	5.341	5.348	5.356
Bulk density (ρ_B) (g/cm^3)	3.924	3.972	4.063	4.156	4.235
Porosity (%)	26.43	25.56	23.93	22.28	20.93

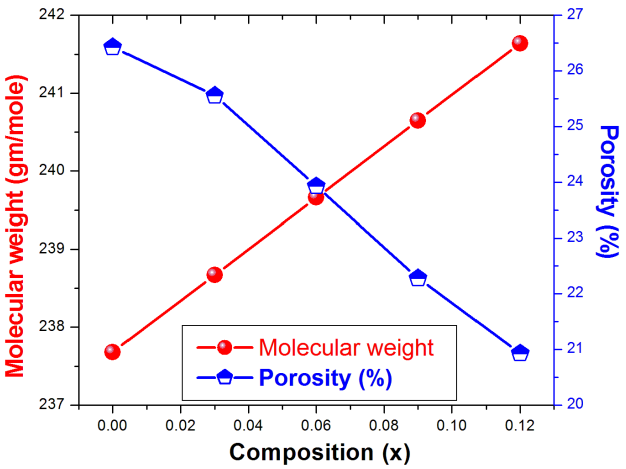

Figure 7. Composition versus molecular weight and porosity of $Ni_{0.4}Zn_{0.6}Y_xFe_{2-x}O_4$ ($x = 0.0$, 0.03, 0.06, 0.09 and 0.12) ferrite nanoparticles.

has a significant effect on ferrite sample micrographs. The growth of grains can be viewed as a struggle between the pushing force for grain boundary progression and the retarding force imposed by the pore. Throughout the sintering process, heat energy produces a force that forces grain boundaries to extend into the pores. This reduces the volume of the pore, making the substance denser. When the pushing force applied to each grain is uniform, the grain size is evenly distributed. Fig. 8 shows FESEM morphology of $Ni_{0.4}Zn_{0.6}Y_xFe_{2-x}O_4$ ($x = 0.0$, 0.03, 0.06, 0.09 and 0.12) ferrite nanoparticles. The topographic visualization confirmed non-uniform grains, agglomerations and well compact structure, similar studies was reported by S. Zahi et. al., The agglomerations in the spinel ferrites were decided by preparation routes, sintering situations and magnetic nature [21]. It was observed that the decreasing of agglomeration in the samples may be due to the doping of feeble yttrium magnetic cations in place of iron magnetic cations and also with the synthesis situation [22]. The EDAX authorizes well pure synthesized ferrites and presence of Ni, Zn, Y, Fe and O, shown in Fig. 9 [23, 24] and posted with their atomic and weight percentages in Table 3.

3.3 VSM analysis

Generally, the magnetic properties of ferrites depend on their chemical composition, grain size, impurities, synthesis route, temperature, $A-B$ exchange interaction and magneto-crystalline anisotropy [25]. The ferrite magnetization is influenced by the super-exchange interactions of $A-B$, $A-A$, and $B-B$ but $A-B$ super-exchange interactions lead over $A-A$ and $B-B$ interactions. The magnetic properties of $Ni_{0.4}Zn_{0.6}Y_xFe_{2-x}O_4$ ($x = 0.0$, 0.03, 0.06, 0.09 and 0.12) powdered particles were determined by a vibrating sample magnetometer. The measured hysteresis loops of the applied field from -20 KOe to $+20$ KOe are shown in Fig. 10. The saturation magnetization (M_s), coercivity (H_c), remanent magnetization (M_r), remanence ratio and magnetic moment/Bohr magneton were extracted from $M-H$ curves

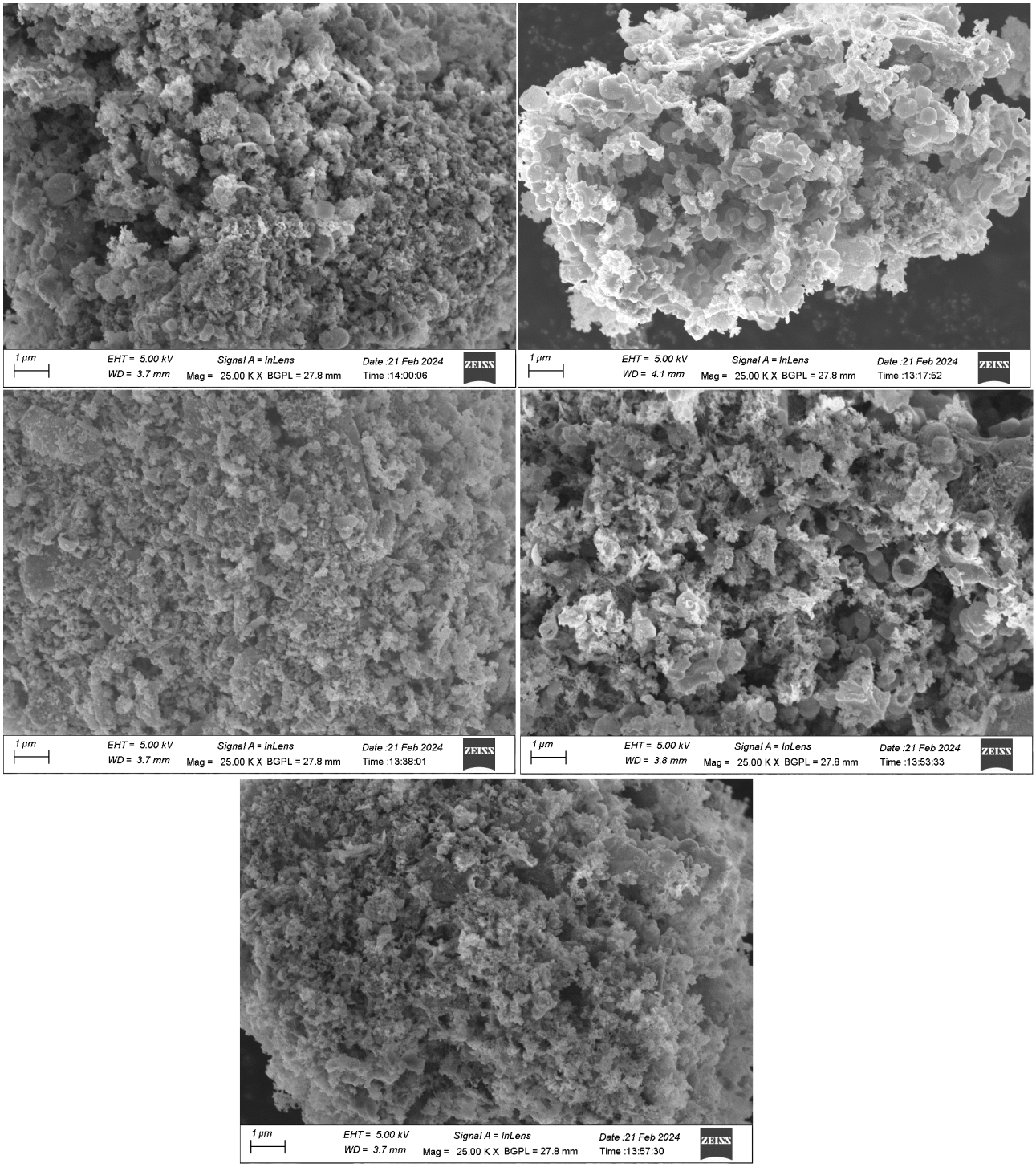

Figure 8. FESEM morphology of $Ni_{0.4}Zn_{0.6}Y_xFe_{2-x}O_4$ ($x = 0.0$, 0.03, 0.06, 0.09 and 0.12) ferrite nanoparticles.

and posted in Table 4. The magnetic moment is evaluated with Eq. (8).

$$\mu_B = \frac{M_w \times M_s}{5585} \tag{8}$$

where, M_w = molecular weight of the sample, M_s = saturation magnetization. A. B. Gadkari et al., reported that the amount of dopant in ferrite has a significant impact on the net magnetic moment of the manufactured nano ferrite particles and their use. The dopants in the Ni-Zn ferrite help to clarify the various behaviour of saturation magnetization. Furthermore, the ionic radii of the dopant elements change the saturation magnetization of the ferrite samples. This article found that pure Ni-Zn ferrite has a higher magnetization than substituted yttrium metal ions. The magnetisation of spinel ferrite particles is modified by lattice defects and surface spin disorder when a magnetic field is applied. From Fig. 11 (a) and (b), it was noticed that saturation magnetization (M_s), magnetic moment (n_B), coercivity (H_c) and remanence magnetization (M_r) declined with Y^{3+} ion concentration. This is due to the replacement of Fe^{3+} ions in

Table 3. The atomic weight composition and constituent elements of $Ni_{0.4}Zn_{0.6}Y_xFe_{2-x}O_4$ ($x = 0.0$, 0.03, 0.06, 0.09 and 0.12) ferrite nanoparticles.

Composition ($x = 0.0$)	Element	Weight (%)	Atomic (%)
$Ni_{0.4}Zn_{0.6}Fe_2O_4$	Y	0.0	0.0
	O	27.64	46.62
	Fe	42.88	26.58
	Ni	12.06	11.54
	Zn	17.42	15.26
TOTAL		**100**	**100**
Composition ($x = 0.03$)	Element	Weight (%)	Atomic (%)
$Ni_{0.4}Zn_{0.6}Y_{0.03}Fe_{1.97}O_4$	Y	5.21	4.45
	O	25.06	29.66
	Fe	39.88	35.23
	Ni	11.59	14.34
	Zn	18.25	16.32
TOTAL		**99.99**	**100**
Composition ($x = 0.06$)	Element	Weight (%)	Atomic (%)
$Ni_{0.4}Zn_{0.6}Y_{0.06}Fe_{1.94}O_4$	Y	8.47	5.72
	O	28.40	36.15
	Fe	31.51	27.89
	Ni	13.05	12.71
	Zn	18.57	17.53
TOTAL		**99.99**	**100**
Composition ($x = 0.09$)	Element	Weight (%)	Atomic (%)
$Ni_{0.4}Zn_{0.6}Y_{0.09}Fe_{1.91}O_4$	Y	10.08	8.25
	O	27.07	32.08
	Fe	29.04	29.85
	Ni	14.25	13.54
	Zn	19.56	16.28
TOTAL		**100**	**99.99**
Composition ($x = 0.12$)	Element	Weight (%)	Atomic (%)
$Ni_{0.4}Zn_{0.6}Y_{0.12}Fe_{1.88}O_4$	Y	12.17	9.57
	O	29.05	33.48
	Fe	23.94	27.15
	Ni	15.89	12.54
	Zn	18.95	17.26
TOTAL		**100**	**100**

Table 4. H_c, M_s, M_r, M_r/M_s, nB values of $Ni_{0.4}Zn_{0.6}Y_xFe_{2-x}O_4$ ($x = 0.0$, 0.03, 0.06, 0.09 and 0.12) ferrite nanoparticles.

Composition (x)	Coercivity H_c (Oe)	Saturation Magnetization M_s (emu/g)	Remanent Magnetization M_r (emu/g)	Remanence Ratio (M_r/M_s)	Magnetic moment (n_B) ($M_{wx}M_s/5585$)
0.0	206	29.19	16.76	0.57	1.24
0.03	164	25.72	14.25	0.55	1.10
0.06	123	23.87	13.32	0.59	1.02
0.09	92	21.26	12.35	0.58	0.92
0.12	56	19.89	11.63	0.58	0.86

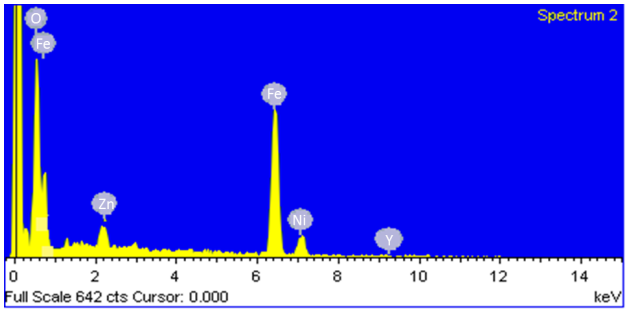

Figure 9. EDX pattern of $Ni_{0.4}Zn_{0.6}Y_xFe_{2-x}O_4$ ($x = 0.03$) ferrite nanoparticles.

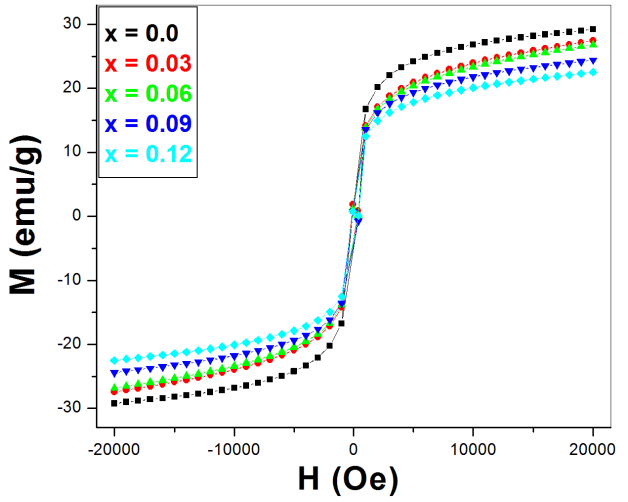

Figure 10. Magnetic Hysteresis (M-H) loops of $Ni_{0.4}Zn_{0.6}Y_xFe_{2-x}O_4$ ($x = 0.0$, 0.03, 0.06, 0.09 and 0.12) ferrite nanoparticles

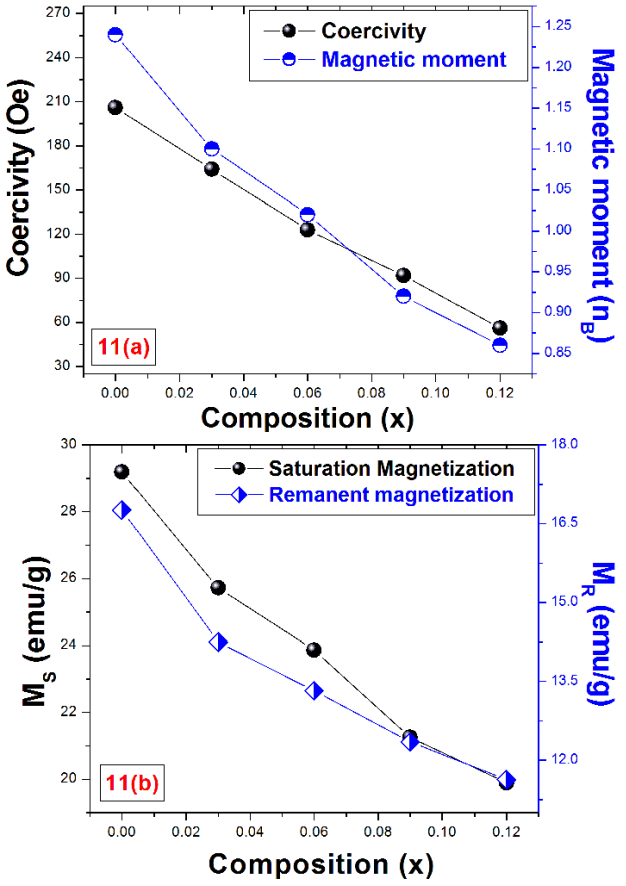

Figure 11. Composition versus (a) coercivity-magnetic moment (b) M_s - M_R of $Ni_{0.4}Zn_{0.6}Y_xFe_{2-x}O_4$ ($x = 0.0$, 0.03, 0.06, 0.09 and 0.12) ferrite nanoparticles.

the *B*-site with paramagnetic Y^{3+} ions, which hold a lesser magnetic moment and also because Y^{3+} ions diminish $A-B$ exchange interactions in the *B*-site [26]. The coercivity is observed to fall with Y^{3+} ion concentration as the particle size is increased (Table 1) because the coercivity is inversely proportional to particle size [26]. The remanence ratio value rises (Table 4) because of the isotropic nature of the prepared samples [27]. Aleena Kiran et al. reported a similar type of study.

4. Conclusion

The sol-get auto-combustion technique is used for the synthesis of various Y-Ni-Zn ferrites. XRD confirmed the single cubic structure without any impurities. The crystallite size, lattice constant, jump lengths, and unit cell volume were noticed to rise as a result of the yttrium substitution. The density values of the synthesized samples showed a significant change with yttrium concentration. It was observed that the X-ray density and bulk density rises, whereas porosity decreases with yttrium substitution. FESEM explained the morphology, agglomerations and

grain size deviations of the samples. It was noticed that the micrographs indicate non-uniform grain size, agglomerations and a densely packed structure on the Ni-Zn ferrite surface. The agglomerations in spinel ferrites can be endorsed to factors such as the preparation route, sintering temperature and magnetic nature of the synthesized samples. The grain size varies, which could be attributed to differences in the doping level of the ferrite. The EDX analysis verified the successful introduction of Y^{3+} ions into Ni-Zn ferrite. The coercivity, saturation magnetization, remanence, and magnetic moment were observed to decrease with yttrium substitution, and it was noted that they are in the range of 206 – 56 Oe, 29.19 – 19.89 emu/g, 16.79 – 11.63 emu/g and 1.24 – 0.86 A-m^2 respectively. In this article it was reported that the samples gave high coercivity values hence the ferrites with high coercivity values are usually treated as hard magnetic materials hence, they used to construct the permanent magnets.

Acknowledgments

The author expresses gratitude to the principal and management of Sreenidhi Institute of Science and Technology for their tremendous support and encouragement.

Authors contributions
Not applicable.

Availability of data and materials
No data was used for the research described in the article.

Conflict of interests
The authors declare that they have no known competing financial interests or personal relationships that could have appeared to influence the work reported in this paper.

References

[1] Y. H. Hou, Y. J. Zhao, Z. W. Liu, H. Y. Yu, X. C. Zhong, W. Q. Qiu, D. C. Zeng, and L. S. Wen. "Structural, electronic and magnetic properties of partially inverse spinel $CoFe_2O_4$: a first-principles study.". *Journal of Physics. D, Applied Physics*, **43**: 445003, 2010. DOI: https://doi.org/10.1088/0022-3727/43/44/445003.

[2] M. A. Ahmed, N. Okasha, and L. Salah. "Influence of yttrium ions on the magnetic properties of Ni–Zn ferrites.". *Journal of Magnetism and Magnetic Materials*, **264**:241–250, 2003. DOI: https://doi.org/10.1016/S0304-8853(03)00212-9.

[3] V. P. Senthil, J. Gajendiran, S. G. Raj, T. Shanmugavel, G. R. Kumar, and C. P. Reddy. "Study of structural and magnetic properties of cobalt ferrite ($CoFe_2O_4$) nanostructures.". *Chemical Physics Letters*, **695**:19–23, 2018. DOI: https://doi.org/10.1016/j.cplett.2018.01.057.

[4] S. Akhter, P. Roy, M. A. Hossain, M. N. I. Khan, and S. S. Sikder. "Influence of yttrium substitution on structural and transport properties of Ni-Zn (Ni.Zn.YFeO) ferrite. ". *Journal of Engineering*, **10**: 45–50, 2019. DOI: https://doi.org/10.1016/S0304-8853(03)00212-9.

[5] W. Zhang, X. Zuo, D. Zhang, C. Wu, S. Ravi, and P. Silva. "Cr^{3+} substituted spinel ferrite nanoparticles with high coercivity. ". *Nanotechnology*, **27**: 245707, 2016. DOI: https://doi.org/10.1088/0957-4484/27/24/245707.

[6] S. Chakrabarty, A. Dutta, and M. Pal. "Effect of yttrium doping on structure, magnetic and electrical properties of nano-crystalline cobalt ferrite. ". *Journal of Magnetism and Magnetic Materials*, **461**:69–75, 2018. DOI: https://doi.org/10.1016/j.jmmm.2018.04.051.

[7] K. Zhang, A. N. Kleit, and A. Nieto. "An economics strategy for criticality–Application to rare earth element Yttrium in new lighting technology and its sustainable availability. ". *Renewable and Sustainable Energy Reviews*, **77**:899–915, 2017. DOI: https://doi.org/10.1016/j.rser.2016.12.127.

[8] J. Petry, R. Komban, C. Gimmler, and H. Weller. "Simple one pot synthesis of luminescent europium doped yttrium oxide Y_2O_3: Eu nano discs for phosphor converted warm white LEDs.". *Nano Scale Advances*, **4**:858–864, 2022. DOI: https://doi.org/10.1039/D1NA00831E.

[9] R. Sharma, P. Thakur, P. Sharma, and V. Sharma. " Ferrimagnetic Ni^{2+} doped Mg-Zn spinel ferrite nanoparticles for high density information storage. ". *Journal of Alloys and Compounds*, **704**:7–17, 2017. DOI: https://doi.org/10.1016/j.jallcom.2017.02.021.

[10] M. B. Khanvilkar, A. K. Nikumbh, R. A. Pawar, N. J. Karale, P. A. Nagwade, D. V. Nighot, and S. P. Panchgalle. "Effect of divalent/trivalent doping on structural, electrical and magnetic properties of spinel ferrite nanoparticles. ". *Engineered Science*, **22**:850, 2023. DOI: https://doi.org/10.30919/es8d850.

[11] M. A. Islam, A. A. Hossain, M. Z. Ahsan, M. A. A. Bally, M. S. Ullah, S. M. Hoque, and F. A. Khan. "Structural characteristics, cation distribution, and elastic properties of Cr^{3+} substituted stoichiometric and non-stoichiometric cobalt ferrites. ". *RSC Advances*, **12**:8502–8519, 2022. DOI: https://doi.org/10.1039/d1ra09090a.

[12] A. A. Momin, R. Parvin, and A. A. Hossain. "Structural, morphological and magnetic properties variation of nickel-manganese ferrites with lithium substitution.". *Journal of Magnetism and Magnetic Materials*, **423**:124–132, 2017. DOI: https://doi.org/10.1016/j.jmmm.2016.09.078.

[13] A. Ahad and A. K. M. Akther Hossain. "Enhancement of microstructural and magnetic properties of high spin Mn substituted nano crystalline Ni–Mn–Cu–Zn ferrites. ". *Heliyon*, **10**, 2024. DOI: https://doi.org/10.1016/j.heliyon.2024.e26050.

[14] P. S. Hedaoo, D. S. Badwaik, S. M. Suryawanshi, and K. G. Rewatkar. "Structural and magnetic studies of Zn doped nickel nanoferrites synthesize by sol-gel auto combustion method.". *Materials Today: Proceedings*, **15**:416–423, 2019. DOI: https://doi.org/10.1016/j.matpr.2019.04.102.

[15] B. Jyothish and J. Jacob. "Al-doped zinc ferrite nanoparticles: Preparation and evaluation of thermal, structural, morphological and anticancer properties.". *Journal of Alloys and Compounds*, **863**:158352, 2021. DOI: https://doi.org/10.1016/j.jallcom.2020.158352.

[16] J. Ferdaus, M. K. Das, A. Dey, B. C. Das, F. Alam, M. Rahaman, and M. S. Bashar. "Influence of Zn-substitution on structural, magnetic, dielectric, and electric properties of Li–Ni–Cu ferrites. ". *Heliyon*, **9**, 2023. DOI: https://doi.org/10.1016/j.heliyon.2023.e21633.

[17] D. V. Kurmude, R. S. Barkule, A. V. Raut, D. R. Shengule, and K. M. Jadhav. "X-ray diffraction and cation distribution studies in zinc-substituted nickel ferrite nanoparticles. ". *Journal of Superconductivity and Novel Magnetism*, **27**:547–553, 2014. DOI: https://doi.org/10.1007/s10948-013-2305-2.

[18] S. G. Kakade, Y. R. Ma, R. S. Devan, Y. D. Kolekar, and C. V. Ramana. "Dielectric, complex impedance and electrical transport properties of erbium (Er^{3+}) ion-substituted nanocrystalline, cobalt-rich ferrite ($Co_{1.1}Fe_{1.9-x}Er_x\ O_4$). ". *Journal of Physical Chemistry C*, **120**:5682–5693, 2016. DOI: https://doi.org/10.1021/acs.jpcc.5b11188.

[19] G. Nabiyouni, M. J. Fesharaki, M. Mozafari, and J. Amighian. "Characterization and magnetic properties of nickel ferrite nanoparticles prepared by ball milling technique.". *Chinese Physics Letters*, **27**: 126401, 2010. DOI: https://doi.org/10.1088/0256-307X/27/12/126401.

[20] K. K. Rama, K. K. Vijaya, and R. Dachepalli. "Structural and electrical conductivity studies in nickel-zinc ferrite.". *Advances in Materials physics and Chemistry*, **28**, 2012. DOI: https://doi.org/10.4236/ampc.2012.23028.

[21] S. Zahi. "Synthesis, permeability and microstructure of the optimal nickel-zinc ferrites by sol-gel route. ". *Journal of Electromagnetic Analysis and Applications*, , 2010. DOI: https://doi.org/10.4236/jemaa.2010.21009.

[22] P. A. Rao, V. Raghavendra, B. Suryanarayana, T. Paulos, N. Murali, P. P. Varma, and K. Chandramouli. "Cadmium substitution effect on structural, electrical and magnetic properties of Ni-Zn nano ferrites.". *Results in Physics*, **19**:103487, 2020. DOI: https://doi.org/10.1016/j.rinp.2020.103487.

[23] Y. Slimani, M. A. Almessiere, A. D. Korkmaz, A. Baykal, A. Manikandan, H. Gungunes, and M. S. Toprak. "Ultrasound-assisted synthesis and magnetic investigations of $Ni_{0.4}Cu_{0.4}Zn_{0.2}Ga_xGd_xFe_{2-2x}O_4$ ($0.00 \leq x \leq 0.04$) nano sized spinel ferrites.". *Applied Physics A*, **128**:593, 2022. DOI: https://doi.org/10.1016/j.ultsonch.2019.05.001.

[24] R. Quhe, J. Zheng, G. Luo, Q. Liu, R. Qin, J. Zhou, and J. Lu. "Tunable and sizable band gap of single-layer graphene sandwiched between hexagonal boron nitride. ". *NPG Asia Materials*, **4**:1–10, 2012. DOI: https://doi.org/10.1038/am.2012.10.

[25] A. A. Sattar, H. M. Elsayed, and A. M. Faramawy. "Comparative study of structure and magnetic properties of micro-and nano-sized $Gd_xY_{3-x}Fe_5O_{12}$ garnet.". *Journal of Magnetism and Magnetic Materials*, **412**:172–180, 2016. DOI: https://doi.org/10.1016/j.jmmm.2016.03.090.

[26] L. George, C. Viji, H. Mathew, and E. M. Mohammed. "Structural, dielectric, magnetic and optical properties of cerium substituted Ni–Zn mixed ferrite. ". *Mater. Sci. Res. India*, **14**:133, 2017. DOI: https://doi.org/10.13005/msri/140208.

[27] S. E. Shirsath, B. G. Toksha, and K. M. Jadhav. "Structural and magnetic properties of In^{3+} substituted $NiFe_2O_4$. ". *Materials Chemistry and Physics*, **117**:163–168, 2009. DOI: https://doi.org/10.1016/j.matchemphys.2009.05.027.